COBEM 2023 27TH INTERNATIONAL CONGRESS OF MECHANICAL ENGENEERING

ABCM Brazilian Society of Mechanical Sciences and Engineering
27th ABCM International Congress of Mechanical Engineering
December 04-08, 2023, Florianópolis-SC, Brazil

# COB-2023-2240
# DEVELOPMENT OF AN EXPERIMENTAL CORRECTION MODEL FOR HORIZONTAL BUOYANCY IN THE TESTING SECTION OF THE CLOSED-CIRCUIT WIND TUNNEL AT UFMG

**Marina Camba Fernandes**
**Guilherme de Souza Papini**
Graduate Program in Mechanical Engineering, Universidade Federal de Minas Gerais, Av. Antônio Carlos, 6627, Pampulha – MG, 31270-901, Brazil.
marinacamba7@gmail.com
papini@demec.ufmg.br

***Abstract.*** *Wind tunnels are classic tools used in the evaluation of aerodynamic forces and moments acting on a body in the flow of air, for example. However, for the data obtained through a tunnel to be reliable, the flow in its test section must be well characterized in order to validate its correspondence with an open-air flow. The present study aims to establish a drag correction model for the horizontal buoyancy effect present in the closed-circuit wind tunnel of the Laboratory of Experimental Aerodynamics at the Federal University of Minas Gerais (UFMG) in order to approximate the results obtained in the test campaigns carried out in it to the results that would be found for an outdoor model. Primary data is obtained through pressure sensors positioned along the central line of the test section to obtain the longitudinal static pressure gradient along it, which is then used for the formulation of the correction model. Finally, a spherical model is tested and the experimental and theoretical results are compared for the validation of the correction model.*

***Keywords:*** *Wind Tunnels, Wall Effects, Horizontal Buoyancy*

## 1. INTRODUCTION

Wind tunnels are very important tools used in aerodynamic, aeroelastic, aeroacoustic studies, among others, during the development of a new aircraft. According to Rasuo (2006), the importance of wind tunnel simulation can be perceived from a comparative analysis of the time spent on aerodynamic tests carried out on particular airplanes in the development, as showed by Figure 1.

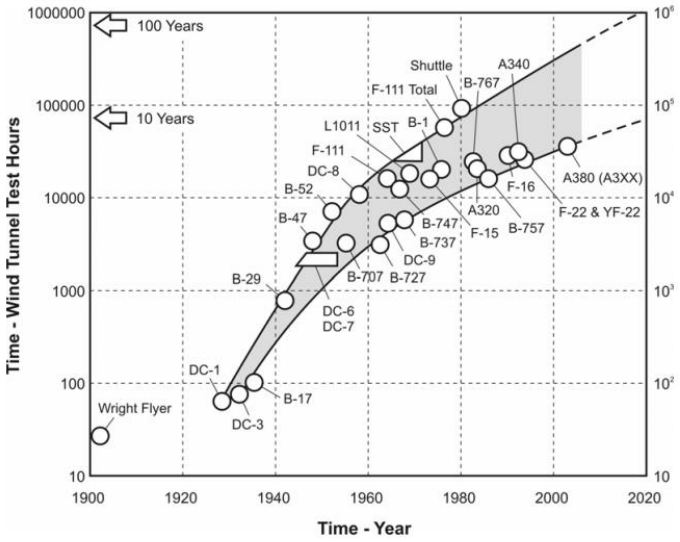


Figure 1 - Wind tunnel testing time of new aircraft in the development phase as a function of aircraft type and year. Source: Rasuo (2006).

Rasuo (2006) claims that the fields containing problems that contribute to inaccuracy in defining wind tunnel corrections can be arranged into four groups: (1) Nonlinearity of the referent equation in the condition of supercritical

flow, (2) Nonlinearity of the boundary conditions of crossflow through ventilated walls and difficulties in predicting or measuring them, (3) Geometric characteristics of the wind tunnel (finite length of the ventilated walls), the entrance to the diffuser and the presence of the testing wake rake and its support, and (4) Boundary layer at the sides of wind tunnel walls, which produces flow deviations as regards the conditions of two-dimensional flow.

The wall interference effects and Reynolds number effects were described as two primary sources of unreliability of the results from wind tunnel tests, according to the Fluid Dynamics Panel Specialists' Meeting, with the objective: Wall Interference in Wind Tunnels, held in London, 19-20 May 1982.

In this way, this work has as main objective to measure and model the effect that the phenomenon of horizontal buoyancy causes in the drag of a model in the test section of the closed-circuit wind tunnel of the Laboratory of Experimental Aerodynamics (LAExp) of UFMG. So that the drag measurements to be carried out can present a high degree of reliability.

## 2. THEORETICAL METHODS

### 2.1 Drag force

For anybody that is immersed in a fluid, for example, air, it is known that regardless of how complex its geometry or flow behavior could be, the aerodynamic forces and moments that act on it come from only two sources: (i) The pressure distribution ($p$) over the surface of the body; (ii) The shear stress distribution ($\tau$) over the surface of the body.

Anderson (1984) claims that the resulting aerodynamic force can be obtained by integrating $p$ and $\tau$ over the entire surface of the body. This force is commonly decomposed into a portion in the direction of the undisturbed flow velocity ($V$), called drag ($D$), and a portion perpendicular to $V$ named lift ($L$).

The drag force depends on both the characteristics of the flow and the shape of the body immersed in it. Therefore, it is often convenient to treat the drag in its dimensionless form called drag coefficient ($C_D$) which is the ratio between the drag force, the body's characteristic area ($A$) and the dynamic pressure of the undisturbed flow.

$$C_D = \frac{D}{\frac{1}{2}\rho V^2 A} \tag{1}$$

It is known that for some shapes - like an airfoil, for example, the drag coefficient is independent of the Reynolds number (i.e., flow velocity), but this is not true for the case of a sphere. Munson et al. (1990) presents a graph that shows de relation between $C_D$ and $Re$ for smooth spheres.

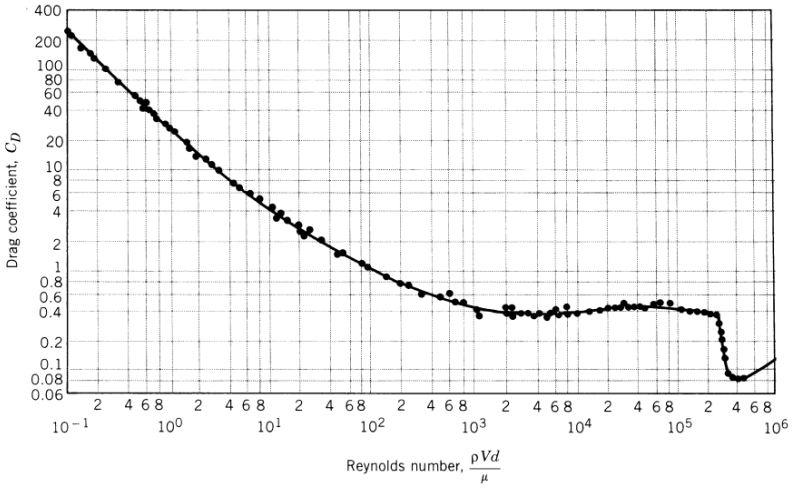


Figure 2 - Effect of Reynolds number on the drag coefficient of a smooth sphere.

### 2.2 Horizontal buoyancy

The conditions under which a model is tested in a wind tunnel are not the same as it would be in the open air. Pope (1999) claims that the longitudinal static pressure gradient present in the test section of a tunnel, whether open or closed, produces excess forces that must be subtracted from the results. The presence of sidewalls in the tunnel causes some disturbances in the flow, called wall effects. For low-speed wind tunnels, one of the most important of which is horizontal buoyancy.

The static pressure gradient along the test section of a wind tunnel appears because of the thickening of the boundary layer along it as shown in Figure 3. According to Pope (1999) this change in pressure produces a force analogous to the hydrostatic force on objects immersed in a stationary fluid and usually produces an increase in drag. Despite being considered negligible for wings and profiles, horizontal buoyancy becomes considerable for blunt bodies, such as fuselages and nacelles. Some tunnels have a small opening angle for the test section, in order to minimize this effect, however this is not the case with the LAExp wind tunnel.

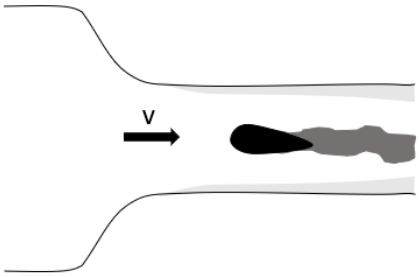


Figure 3 – Boundary-layer thickening along test section.

All closed-circuit wind tunnels that have a test section of constant transversal area experience a static and dynamic pressure variation in the test section axis, that is resulting from the boundary layer thickening along the axis of the section and consequent decrease in the jet area. What happens is that the static pressure is normally more negative as it approaches the exit cone, so the model is "pushed" backwards (Pope, 1999).

The magnitude of the static pressure gradient must be measured experimentally for each tunnel. The equation that Pope (1999) proposes to estimate drag due to horizontal buoyancy for the two-dimensional case considers the static pressure differential between two points and the average area of the model between the same points, of the form:

$$D_B = \int_0^l S(x)p'(x)dx \tag{2}$$

where S denotes the model front area and $p'(x) = \frac{dp}{dx}$.

Considering a constant pressure gradient, and the effect of jet "squeezing" on boundary layer thickening along the test section, Glauert (1933) proposed the following equation to estimate drag due to horizontal buoyancy:

$$D_B = -\frac{\pi}{2}\lambda_2 t^2 \frac{dp}{dl} \tag{3}$$

where $\lambda_2$ denotes a 2D factor and $t$ denotes the model's maximum thickness.

Analogously, the expression for drag on a three-dimensional body is given by:

$$D_B = -\frac{\pi}{4}\lambda_3 t^3 \frac{dp}{dl} \tag{4}$$

where $\lambda_3$ denotes a 3D factor presented in Figure 4.

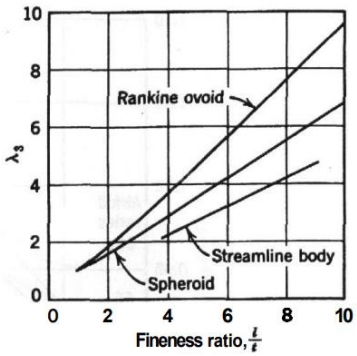


Figure 4 – Horizontal buoyancy shape factor. Source: Pope (1999).

## 3. EXPERIMENTAL METHODS

## 3.1 Instrumentation

### 3.1.1 LAExp Closed-Circuit Wind Tunnel

The UFMG closed-circuit wind tunnel (CCWT), whose project was completed in 2006 is the largest wind tunnel in the campus. It was built entirely in metal and operates between 0 and 90 $m/s$, with its most reliable operating range being between 20 and 70 $m/s$. It is equipped with a Siemens D-91056 ERLANGEN electric motor. The test section of the tunnel is 3 $m$ long and has a cross section in the shape of an irregular octagon as shown in Figure 5 (values in millimeters).

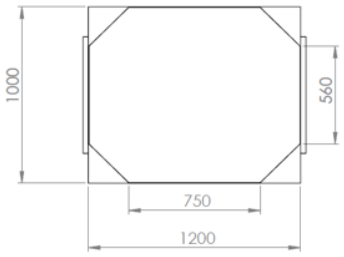


Figure 5 - CCWT test section cross section. Source: Valle (2006).

### 3.1.2 Pitot tube

The Pitot tube used was the L type, with an ellipsoidal head, a total pressure inlet and 6 orifices for static pressure. Body made of stainless steel, as shown in Figure 6.

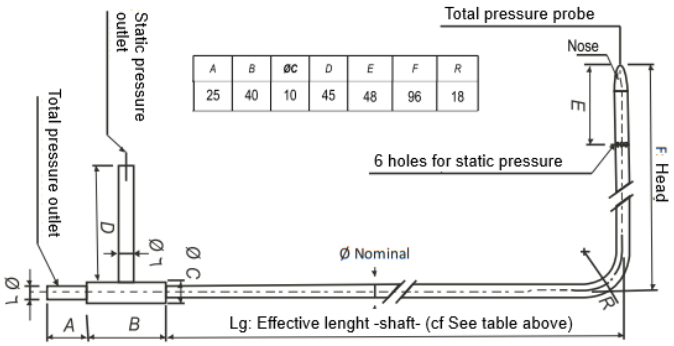


Figure 6 – Pitot tube L type used in the experiment. Source: Instrutemp (translated).

### 3.1.3 ScaniValve

To read the pressure data obtained through the Pitot tubes and transform them into digital signals, the LAExp has a set of pressure transducers ScaniValves totaling sixty-four channels for capillary tubes as shown in Figure 7. The transducer has an ethernet cable output, the pressure sensors are temperature compensated and work in the range of 0 to 5 $MPa$.

Figure 7 - ScaniValves pressure scanners at LAExp.

### 3.1.4 Sphere model and drag acquisition test bench

The sphere used in the experiment was a pool ball with a diameter of $54\ mm$ and a hole measuring $2\ mm$ in diameter to fit a metal rod. A wooden and metal bench was built to connect the load cell to the sphere and position it in the center of the test section. As shown in the following scheme.

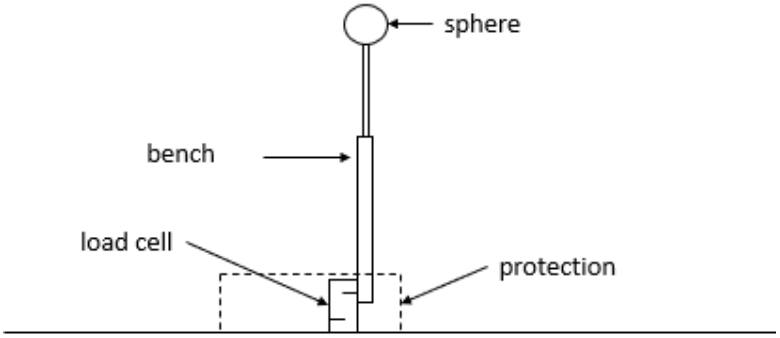


Figure 8 – Drag acquisition test bench.

The load cell is a transducer which converts force into a measurable electrical output. The operating range of this equipment is $0$ to $5\ V$ and its calibration was performed using an object with a known weight attached to the centerline of the sphere using a wire and a sheave. A protective structure was also installed so that the wind would not directly hit the load cell.

## 3.2 Tests Procedure

### 3.2.1 Longitudinal static pressure gradient

For this experiment, the instruments described in sections 3.1.2 and 3.1.3 will be used. The first experimental procedure consists of fixing a Pitot tube at the test section entrance (this tube is originally used to determine the flow velocity in the test section) as a velocity reference, and using a pivoting Pitot tube that will be positioned at four points along the center line of the test section to obtain the static pressure at each of these points in order to obtain a curve of static pressure versus velocity for each point and subsequently a curve of static pressure gradient for each speed. The Figure 9 represents this scheme.

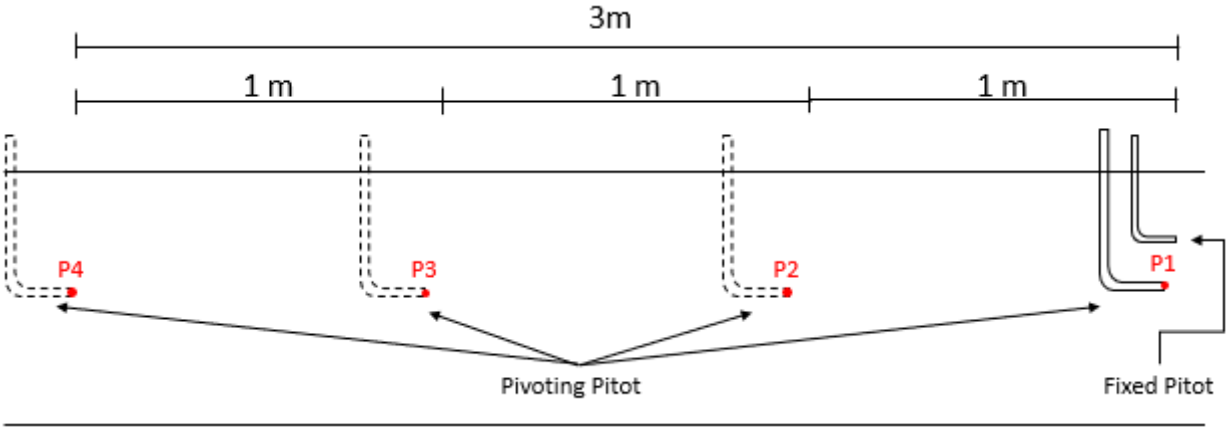


Figure 9 - Experiment 1: Longitudinal static pressure gradient.

### 3.2.2 Drag coefficient for a sphere

The second experiment aims to obtain the drag coefficient for a sphere through the CCWT and further correct it for the buoyancy effect. For this purpose, the devices described in section 3.1.4 was used, as shown in Figure 10. Once the load cell is aligned with the horizontal axis, direct reading of the drag force is possible. The drag force versus streamline velocity curve was acquired for the assembly, in addition the same curve was acquired for the bench alone, and finally

this curve was subtracted from the first one. The resulting curve represents only the drag force due to the sphere through which it was also possible to obtain the drag coefficient of the model using Equation 1.

Figure 10 - Experiment 2: Drag coefficient for a sphere.

## 4. RESULTS AND DISCUSSION

### 4.1 Longitudinal static pressure gradient

The values obtained for static pressure for each speed at each point shown in Figure 11 are shown in the graph of the Figure 11.

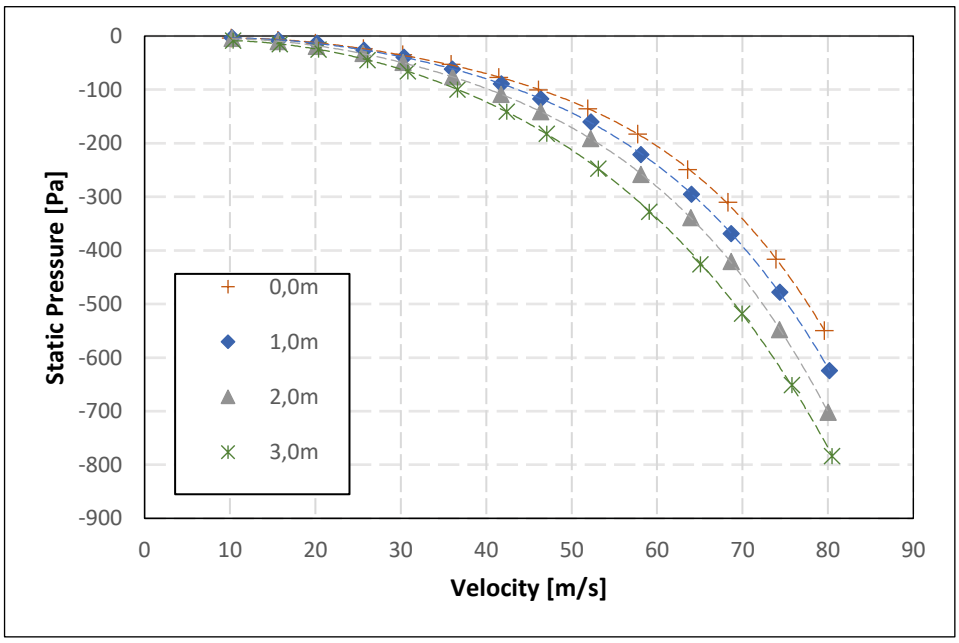


Figure 11 – Static pressure versus velocity.

From the graph above it is possible to observe the static pressure drop with velocity. It is also possible to see that for the same velocity there is also a drop in static pressure as the flow progresses within the test section as expected. As it was not possible to guarantee that the data obtained were always at the same velocity points, the Excel curve fitting tool was used for a fourth-degree polynomial for each curve, with a minimum adjustment coefficient of $R^2 = 0{,}9999$.

From the equations of the adjustment curves, it was possible to obtain the static pressure gradient curves by position in the test section for each velocity value. The Figure 12 shows these curves for some values in the typical working speed range of the CCWT (10 to 70 $m/s$).

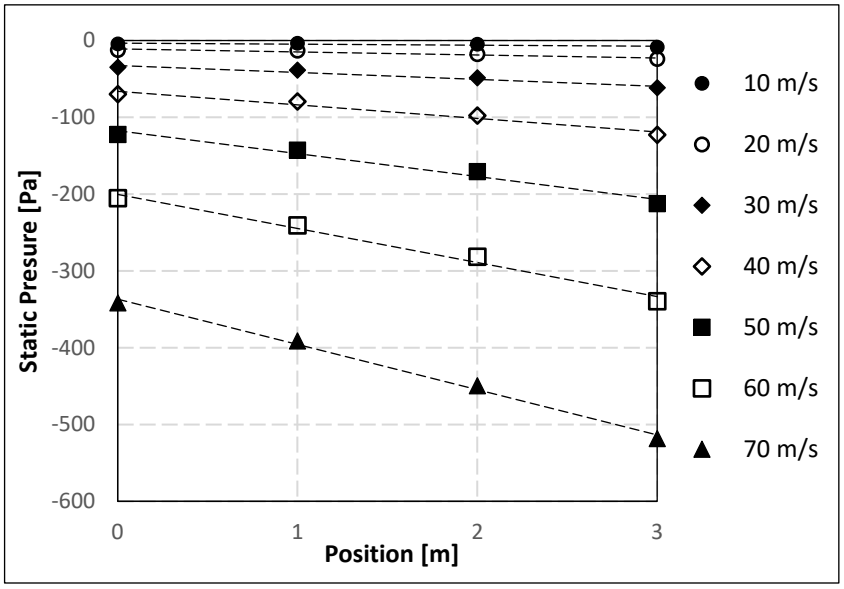


Figure 12 - Longitudinal static pressure gradient.

Again, Excel's curve fitting tool was used, this time for first-degree polynomials, to obtain the equation that relates static pressure with position within the test section. The adjustment coefficient varied between $R^2 = 0{,}9254$ for the lowest speed and $R^2 = 0{,}9946$ for the highest. Finally, from the derivative of each curve, it was possible to obtain the graph that relates the longitudinal static pressure gradient in the test section with the flow inlet velocity.

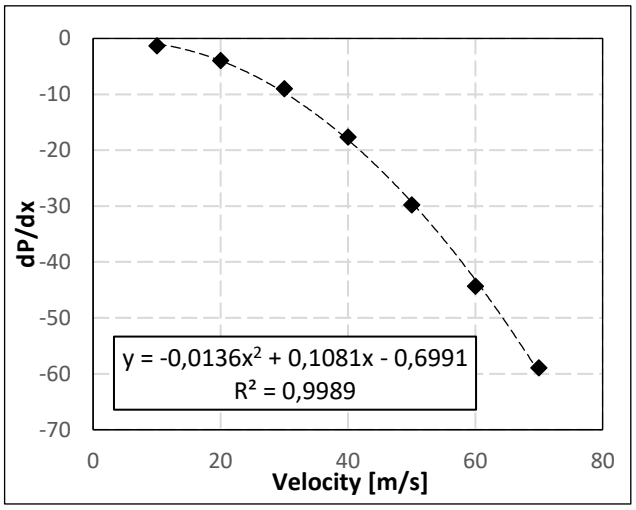


Figure 13 - Longitudinal static pressure gradient by velocity.

Therefore, exclusively for the CCWT of LAExp, there is the equation:

$$\frac{dp}{dl}(V) = -0{,}0136V^2 + 0{,}1081V - 0{,}6991 \tag{5}$$

### 4.2 Horizontal buoyancy correction

Section 4.1.1 presented an equation that relates $\frac{dp}{dl}$ with the undisturbed flow velocity. Thus, substituting Equation 5 in Equation 4, we obtain:

$$D_B = -\frac{\pi}{4}\lambda_3 t^3(-0{,}0136V^2 + 0{,}1081V - 0{,}6991) \tag{6}$$

Equation 6 is the buoyancy correction factor for CCWT of LAExp. As seen in section 2.1, sometimes it is convenient for a body that its drag is treated in its dimensionless form, which for some cases does not depend on the flow velocity, so it is also convenient that the correction for horizontal buoyancy in a wind tunnel is presented in that way. Substituting Equation 6 in Equation 1, one can obtain the buoyancy correction factor for drag coefficient:

$$C_{D_B} = \frac{-\frac{\pi}{4}\lambda_3 t^3(-0{,}0136V^2 + 0{,}1081V - 0{,}6991)}{\frac{1}{2}\rho V^2 A} \tag{7}$$

### 4.2.1 Corrected drag coefficient for a sphere

Applying Equation 7 to the case of a $54\ mm$ diameter smooth sphere of and using the velocities reached in the second experiment, it was possible to obtain the curve of $C_{D_B}$ versus $V$ for the test, shown in Figure 14, where the correction factor for the drag coefficient is shown in drag counts ($1\Delta C_D = 0{,}0001 C_D$).

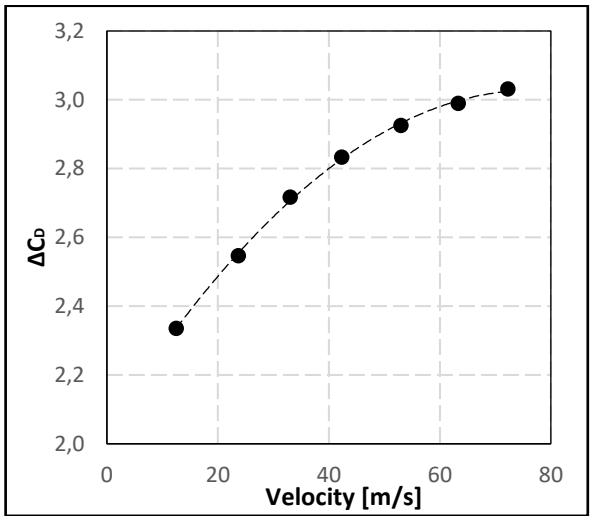


Figure 14 - Correction factors for drag coefficient.

For the representation of the reference data for the drag coefficient on smooth spheres shown in Figure 2, the approximation proposed by Morrison (2013) was used for plotting it along with the results obtained through the CCWT. Finally, applying the methodology described in section 3.2.2, drag data were acquired for points within the CCWT typical working speed range. Figure 15 shows both the raw data obtained in the test and the corrected data. The corresponding values are presented in Table 1.

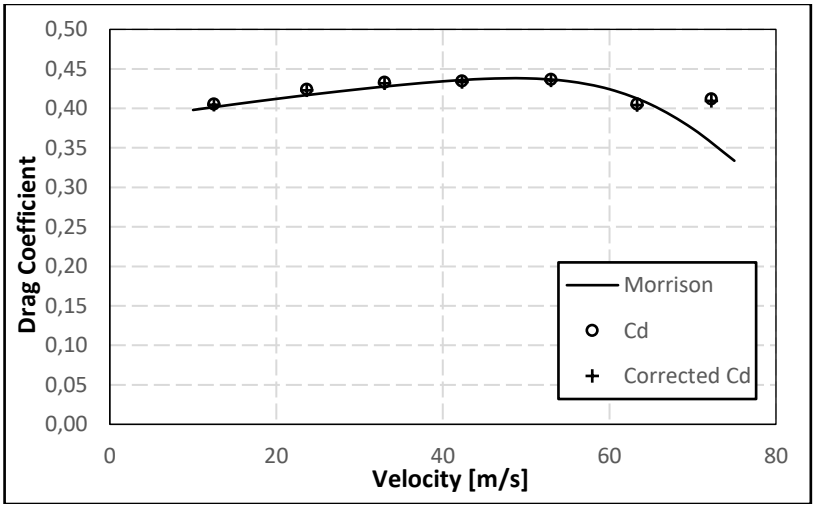


Figure 15 - Raw and treated data for drag coefficient at CCWT.

Table 1 - Values for raw and treated data along with relative errors at CCWT.

| Velocity [m/s] | Cd | | | Relative error | |
|---|---|---|---|---|---|
| | Morrison | Raw | Corrected | Raw | Corrected |
| 12,50 | 0,40161 | 0,40544 | 0,40450 | 0,95% | 0,72% |
| 23,65 | 0,41677 | 0,42373 | 0,42271 | 1,67% | 1,43% |
| 33,00 | 0,42766 | 0,43271 | 0,43163 | 1,18% | 0,93% |
| 42,30 | 0,43591 | 0,43432 | 0,43319 | -0,37% | -0,63% |
| 52,96 | 0,43653 | 0,43649 | 0,43532 | -0,01% | -0,28% |
| 63,32 | 0,41228 | 0,40529 | 0,40409 | -1,70% | -1,99% |
| 72,24 | 0,35675 | 0,41172 | 0,40919 | 15,41% | 14,70% |

It is possible to observe that the results had a good correspondence with the reference data, showing a slight tendency to overestimate the values, which is expected since the wall effects tend to increase the drag for the tested models.

For speeds close to $70\,m/s$ it was noticed that both the test setup and the CCWT structure itself showed considerable vibration, which made it difficult to acquire drag and velocity data and caused them to have a large dispersion.

## 5. CONCLUSION

The results presented in the previous sections show that it was possible to obtain a model for the correction of the horizontal buoyancy effect for the CCWT of LAExp. Section 4.1.2 shows that the correction factor has reduced values when the tested model has a small frontal area, and this proved to be positive since the difference between the results obtained in the tunnel and the reference values was small.

For the data obtained in CCWT tests to become even more reliable, it is recommended that the correction model presented in the present work be also validated for models with a larger frontal area and that other relevant correction factors, such as solid blockage and wake blockage are also modeled. Also, the work speed range can be increased if the CCWT vibration issues are corrected.

## 6. ACKNOWLEDGEMENTS

We thank the Uai Sô, Fly! Team, for kindly loaning their load cell, calibrator, and data acquisition system. We also thank the student Ana Clara Fernandes de Moraes for all the manual and technical help during the experiments.

"This study was financed in part by the Coordenação de Aperfeiçoamento de Pessoal de Nível Superior - Brasil (CAPES) - Finance Code 001"

## 7. REFERENCES

Anderson, J. D. *Fundamentals of Aerodynamics*. 5th edition. McGraw-Hill, 2011.

Glauert, H., *Wind Tunnel Interference on Wings, Bodies and Airscrews*. Aeronautical Research Committeee, 1933.

Instrutemp. *Planilha de dados técnicos*.

Morrison, A., *An Introduction to Fluid Mechanics*. Cambridge University Press, NY, 2013.

Munson, B. R., Young, D. F., and Okiishi, T. H., *Fundamentals of Fluid Mechanics*, Wiley, NY, 1990.

Pope, A., Barlow, J.B.; Era, W.H., *Low Speed Wind Tunnel Testing*, 3rd edition. John Wiley & Sons, 1999.

Rasuo, B. *On Status of Wind Tunnel Wall Correction*. 25th International Congress of the Aeronautical Sciences, ICAS, 2006.

Valle, R.M. *Aquisição do Primeiro Túnel de Vento de Pesquisa e Desenvolvimento de Produtos do Estado de Minas Gerais.* Relatório Final, 2006.

## 8. RESPONSIBILITY NOTICE

The authors are the only responsible for the printed material included in this paper.